

# Feasibility study of $CP$ Violation in $\tau \rightarrow K_S \pi \nu_\tau$ decays at STCF

Haoyu Sang<sup>1,2</sup> Xiaodong Shi<sup>1,2</sup> Xiaorong Zhou<sup>1,2</sup> Xianwei Kang<sup>3,4</sup> Jianbei Liu<sup>1,2</sup>

<sup>1</sup> State Key Laboratory of Particle Detection and Electronics, Hefei 230026, People's Republic of China

<sup>2</sup> University of Science and Technology of China, Hefei 230026, People's Republic of China

<sup>3</sup> Key Laboratory of Beam Technology of Ministry of Education, College of Nuclear Science and Technology, Beijing Normal University, Beijing 100875, People's Republic of China

<sup>4</sup> Beijing Radiation Center, Beijing 100875, China

We report a  $CP$  sensitivity study in  $\tau \rightarrow K_S \pi \nu_\tau$  decays at future Super Tau Charm Facility. With an integrated luminosity of  $1 \text{ ab}^{-1}$  at  $\sqrt{s} = 4.26 \text{ GeV}$ , the statistical sensitivity for the  $CP$  violation is determined to be of order  $9.7 \times 10^{-4}$  by measuring the decay-rate difference between  $\tau^+ \rightarrow K_S \pi^+ \bar{\nu}_\tau$  and  $\tau^- \rightarrow K_S \pi^- \nu_\tau$ . The analysis is performed under a reliable fast simulation software package which can describe the detector response and change the responses flexibly. Furthermore, the energy-dependent efficiencies for reconstructing  $\tau \rightarrow K_S \pi \nu_\tau$  are presented in this analysis and the expected  $CP$  sensitivity is proportional to  $\sqrt{\mathcal{L}}$  in the energy region of  $4.0 \sim 5.0 \text{ GeV}$ , and the sensitivity of  $CP$  violation is of order  $3.1 \times 10^{-4}$  with  $10 \text{ ab}^{-1}$  integrated luminosity in this energy region.

## I. INTRODUCTION

The standard Cabibbo-Kobayashi-Maskawa (CKM) matrix [1, 2] can accommodate  $CP$  violation in a natural way with a complex phase in the quark mixing sector. Experimentally, the  $CP$  violation (CPV) has been observed in the meson sector, firstly in  $K$  meson [3–5], subsequently in  $B$  meson [6–11] and most recently in charm meson decays [12], and all results to date are consistent with the predictions of the CKM mechanism in the Standard Model (SM). However, the origin of  $CP$  violation has remained as an unsolved problem as it is not clear if CKM mechanism is the unique source. The matter-antimatter asymmetry of the Universe [13, 14] indicates that there must be non-SM  $CP$  violation sources, and such additional sources are indeed incorporated in many extensions of the SM [15, 16]. Currently,  $CP$  violation has not yet been observed in the baryon as well as the lepton sector, and any significant observation would be a clear indication of physics beyond the SM. In an intriguing scenario [17], the baryogenesis is argued to be mainly driven by the leptogenesis, and then  $CP$  violation is required in leptodynamics. Thus exploration of CPV in lepton sector does provide a different and complementary landscape, at least. Among the lepton sector,  $\tau$  decay is a good place to seek for CPV either within or beyond SM [18–22], since i) it has abundant hadronic decay channels with sizable branching ratios, and ii) half part of the matrix element is purely electroweak and the involved hadrons are generated by quark-antiquark pairs, such that they are factorized, exempting from complicity of pure hadronic decay.

In this work, we will concentrate on the specific channel  $\tau \rightarrow K_S \pi \nu_\tau$ , due to several reasons: (1)  $CP$  violation and the related New Physics (NP) searches; (2) measurements of form factors and extraction of  $|V_{us}|$  element in CKM matrix; (3) the impact of intermediate resonances and non-perturbative QCD. These will be discussed in more detail in the following section. Meantime,

this channel will be studied as a calibration to perform the optimization of detector design.

Our paper is organized as follows: In Sec. 2, we elaborate the physical significance for investigating the channel  $\tau \rightarrow K_S \pi \nu_\tau$ . In Sec. 3 the detector concept for STCF is introduced as well as the MC samples used for this study. The event selection for tag channel and signal channel which are  $\tau^+ \rightarrow e/\mu \nu \nu$  and  $\tau^- \rightarrow K_S \pi^- \nu$ , respectively, is presented in Sec. 4. Section 5 focuses on the optimization of detector response and Sec. 6 the statistical results. Finally, we conclude in Sec. 7.

## II. DISCUSSIONS ON THE PHYSICAL SIGNIFICANCE OF THE CHANNEL $\tau \rightarrow K_S \pi \nu_\tau$

Within the SM, there is no direct  $CP$  violation in hadronic  $\tau$  decays at the tree level in weak interaction, however, the well-measured  $CP$  asymmetry in  $K_L \rightarrow \pi^\pm l^\pm \nu$  produces a difference in  $\Gamma(\tau^+ \rightarrow K_L \pi^+ \bar{\nu})$  vs.  $\Gamma(\tau^- \rightarrow K_L \pi^- \nu)$  due to the  $K^0 - \bar{K}^0$  oscillation. The same asymmetry also appears in  $\Gamma(\tau^+ \rightarrow K_S \pi^+ \bar{\nu})$  vs  $\Gamma(\tau^- \rightarrow K_S \pi^- \nu)$ , and is calculated to be [23, 24]

$$\begin{aligned} A_{CP}(\tau \rightarrow K_S \pi \nu) &= \frac{\Gamma(\tau^+ \rightarrow K_S \pi^+ \bar{\nu}_\tau) - \Gamma(\tau^- \rightarrow K_S \pi^- \nu_\tau)}{\Gamma(\tau^+ \rightarrow K_S \pi^+ \bar{\nu}_\tau) + \Gamma(\tau^- \rightarrow K_S \pi^- \nu_\tau)} \\ &= (0.36 \pm 0.01)\%, \end{aligned} \quad (1)$$

where the convolution with efficiency has been taken into account. Experimentally, BABAR experiment has found evidence for  $CP$  violation in  $\tau$  decays [25]

$$A_{CP}(\tau \rightarrow K_S \pi \nu[\geq 0\pi^0]) = (-0.36 \pm 0.23 \pm 0.11)\%, \quad (2)$$

and there is a 2.8 standard deviation difference from the theoretical prediction in Eq. (1). In SM the  $K^0 - \bar{K}^0$  oscillation leads to the same value of  $CP$  asymmetry for inclusion of any  $\pi^0$ s. Motivated by such  $CP$  anomaly,

various NP scenarios are proposed, *e.g.*, by introducing the non-standard tensor interaction [26, 27], where in Ref. [27] even the large angular-weighted  $CP$  asymmetry is predicted. However, in Ref. [28] the authors pointed out that the tensor contribution therein are overestimated due to lacking of the well-known Watson theorem of final-state interaction (often used in the analysis of hadron spectrum, *e.g.*, in Ref. [29]). As a result, a very large value of the imaginary part of the Wilson coefficient for the tensor operator would be required to accommodate the  $CP$  anomaly, which in turn, contradicts with the bound from neutron electric dipole moment (EDM) and  $D - \bar{D}$  mixing, unless NP occurs below the electroweak breaking scale. This standpoint is adopted later by Refs. [30, 31], and especially, Ref. [31] finds that once the combined constraints from the branching ratio and decay spectrum are included, both of the models used there fail to explain the experimental CPV even without recurring to the aforementioned bounds. As a dramatic reversal, Ref. [32] points out that the tensor operator used in Ref. [28] corresponds to only a specific way of imposing gauge invariance, and instead, the new type of tensor operator can account for the  $CP$  anomaly as well as the long-standing “ $|V_{us}|$ ” puzzle, by evading bounds from the neutron EDM. Thus confirmation of the BABAR result on the  $CP$  anomaly is necessary as a forward step to approach any conclusive statement on NP signal. We stress the importance of precision here. Moreover, as discussed in Ref. [33], the probing of  $A_{CP}(\tau \rightarrow K\pi\nu)$ ,  $A_{CP}(\tau \rightarrow K2\pi\nu)$  and  $A_{CP}(\tau \rightarrow K3\pi\nu)$  separately can help to establish the existence of new dynamics since the global  $CP$  violation as expressed in Eq. (2) are often much reduced, and one needs to understand the basis of the observed data on  $\tau^- \rightarrow K_S\pi^-\nu[\geq 0\pi^0]$  vs.  $\tau \rightarrow K\pi\nu$ ,  $\tau \rightarrow K2\pi\nu$  and  $\tau \rightarrow K3\pi\nu$ . In SM, the same  $CP$  asymmetry holds for the decay including any number of  $\pi^0$  meson, due to the sole source by  $K^0 - \bar{K}^0$  oscillation. But the situation will change in the presence of NP, as shown in Refs. [34] and [35], where the two-Higgs Doublet Model is used to show its influence on the different observable sets for the channels  $\tau \rightarrow K\pi\pi\nu_\tau$  and  $\tau \rightarrow K\pi\nu_\tau$ . Certainly, more complicated impact of resonances appear in the multibody channels, and more statistic data is needed in this case. We also note that in the four- and five-body decays, one can also access to the CPV by T-odd observables [36].

Apart from the above BABAR measurement, CLEO [37] and Belle [38] collaboration focus on the  $CP$  violation that could arise from a charged scalar boson exchange [39], and this type of  $CP$  violation can be detected as a difference in the  $\tau$  decay angular distributions. The results are found to be compatible with zero with a precision of  $\mathcal{O}(10^{-3})$  in each mass bin [38]. In all these experimental measurements, the statistical uncertainty is at the same level of  $\mathcal{O}(10^{-3})$  and the current experimental sensitivity cannot make a conclusion on the  $CP$  from  $\tau$  decay. Therefore a higher-precision result is highly required for clarifying

the New Physics feature.

In order to capture the faint NP signal, or instead, to constrain the NP model, the accurate knowledge of form factor is also an essential input, as already seen in Refs. [27, 30]. The  $\tau \rightarrow K_S\pi\nu$  decay in the SM is described by the vector and scalar form factors. The vector form factor receives mainly the contribution of  $K^*(892)$ , and  $K^*(1410)$  is also needed in the higher-energy region tail, while for the scalar one there is no clear dominance of single resonance. Currently the most sophisticated description of the form factors are obtained by the model-independent dispersive representation imposing constraints from chiral symmetry and their asymptotic QCD behaviour [40–42]. However, other descriptions are available, *e.g.* in Refs. [35] and [43]. In the former, the form factors are calculated up to one-loop level using the chiral Lagrangian. The resulting shape differs from the dispersive one, and in our opinion, such difference can be attributed to the perturbative vs non-perturbative treatment. In the latter one [43], experimentalist aims to achieve a satisfactory description of data in a phenomenological way, and then a superposition of Breit-Wigner functions is used. As already commented in Ref. [28], the resulting phase does not vanish at threshold and also violates the Watson theorem before the inelasticity sets in. As a consequence, it also violates the unitarity condition. However, all these variants of form factor describe equally well the data for the total mass spectrum. The  $P$ -wave form factor agrees and  $S$ -wave form factor can differ dramatically in different model calculations. A partial-wave analysis will certainly helps to pin down this issue, which again needs more high-quality data. This point has been noted by Belle collaboration [43]: the future more data on the invariant mass spectrum of  $K_S\pi$  combined with the angular analysis will elucidate the nature of scalar form factor and check various theoretical approach. We also notice that by precisely measuring the channel  $\tau \rightarrow K_S\pi\nu$ , i) the  $|V_{us}|$  element can be determined, which is worth to do, at least, as another cross check of its extraction from exclusive decay mode, and for a review see *e.g.*, Ref. [21]; ii) the peculiar and incomprehensible data points in bins 5-7 for the  $K_S\pi$  mass spectrum are hopeful to clarify [30]; iii) the resonance parameters (mass and width) can be determined, which itself is an important topic of the hadron spectrum, with assisting us to understand more on the strong impact of intermediate resonances and their interference. We also notice that the large strong phase will be rendered in the resonance region, which together with the weak phase is a requisite for generating CPV. Again as stressed, to make a conclusive remark one needs “precision” in the measurement. We indeed need to enter into the “precision” era.

Fortunately, the Super Tau Charm Facility(STCF) is a scientific project proposed for high energy physics frontier in China, which is hopeful to reexamine all the problems discussed above, and especially focusing on the CPV measurement and the decay spectrum. It is a symmetry

electron-positron beam collider designed to provide  $e^+e^-$  interactions at a center-of-mass (c.m.) energy  $\sqrt{s}$  from 2.0 to 7.0 GeV. The peaking luminosity is expected to be  $0.5 \times 10^{35} \text{ cm}^{-2}\text{s}^{-1}$  at  $\sqrt{s} = 4.0 \text{ GeV}$ , and the integrated luminosity per year is  $1 \text{ ab}^{-1}$ . For more details, see Refs. [44, 45]. The peaking cross section for  $\tau$  pair production  $e^+ + e^- \rightarrow \tau^+ + \tau^-$  is around 4.26 GeV, yielding  $3.5 \times 10^9$   $\tau$  pairs per year, which can reduce statistical uncertainty for the  $\tau \rightarrow K_S \pi \nu$  significantly and provide the results with a sensitivity compatible with theoretical prediction. Last but not least, to make the best of the large statistic, it is necessary to have a compatibly sophisticated detector at STCF to precisely detect and measure particles, where the channel  $\tau \rightarrow K_S \pi \nu$  studied here can serve as a benchmark physics process to perform the optimization of detector design.

### III. DETECTOR AND MC SIMULATION

The STCF detector is a general designed detector for  $e^+e^-$  collider which includes a tracking systems composed of the inner and outer trackers, a particle identification (PID) system with  $3\sigma$   $K/\pi$  separation up to 2 GeV/c, an electromagnetic calorimeter (EMC) with an excellent energy resolution and a good time resolution, a super-conducting solenoid and a muon detector (MUD) that provide good  $\pi/\mu$  separation. The detailed conceptual design for each sub-detector, the expected detection efficiency and resolution can be found in Ref. [47]. Currently, the STCF detector and the corresponding offline software system are under research and development (R&D) [46], and it is necessary to have a reliable simulation tool which can access the physics reaches. A fast simulation tool for STCF is therefore developed [47], which takes the most common event generator as input to perform a fast and realistic simulation. The simulation includes resolution and efficiency responses for tracking of final state particles, PID system and kinematic fit related variables. Besides, the fast simulation also provide some functions for adjusting performance of each subsystem which can be used to optimize the detector design according to physical requirement.

MC samples normalized of  $1 \text{ ab}^{-1}$  luminosity at  $\sqrt{s} = 4.26 \text{ GeV}$  are simulated. The MC events from  $e^+e^- \rightarrow l^+l^-$  ( $l = e, \mu$ ) and  $e^+e^- \rightarrow \gamma\gamma$  are generated with BABAYAGA [49], and for  $e^+e^- \rightarrow \text{hadrons}$  we use LUNDALW [50]. The  $e^+e^- \rightarrow \tau^+\tau^-$  process is generated with KKMC [51] which implement the TAUOLA to describe the production of  $\tau$  pair. Passage of the particles through the detector is simulated by the fast simulation software [47].

The signal process  $\tau \rightarrow K_S \pi \nu_\tau$  are generated with vector and scalar configurations of  $K_S \pi$  and the decay am-

plitude is described by:

$$\frac{d\Gamma}{d\sqrt{s}} \propto \frac{1}{s} \left(1 - \frac{s}{m_\tau^2}\right)^2 \left(1 + \frac{2s}{m_\tau^2}\right) P(s) \times \left\{ P^2(s) |F_V|^2 + \frac{3(m_{K_S}^2 - m_\pi^2)^2 |F_S|^2}{4s(1 + \frac{2s}{m_\tau^2})} \right\}, \quad (3)$$

where  $s$  is the squared invariant mass of  $K_S \pi$ .  $m_\tau, m_{K_S}$  and  $m_\pi$  are the mass of  $\tau, K_S$  and  $\pi$  [52].  $P(s)$  is the momentum of  $K_S/\pi$  in the  $K_S \pi$  rest frame, given by:

$$P(s) = \frac{\sqrt{(s - (m_{K_S} + m_\pi)^2)(s - (m_{K_S} - m_\pi)^2)}}{2\sqrt{s}}. \quad (4)$$

The  $F_S$  and  $F_V$  are the scalar and vector form factors to parameterize the amplitudes of  $K_0^*(800)$ ,  $K^*(892)$  and  $K^*(1410)$ :

$$F_S = a_{K_0^*(800)} \cdot BW_{K_0^*(800)}, \quad (5)$$

$$F_V = \frac{BW_{K^*(892)} + a_{K^*(1410)} \cdot BW_{K^*(1410)}}{1 + a_{K^*(1410)}}, \quad (6)$$

where BW denotes Breit-Wigner function, and  $a_{K_0^*(800)}$  and  $a_{K^*(1410)}$  are the coupling constant as presented in Ref. [53].

### IV. EVENT SELECTION AND ANALYSIS

We select signal events with one  $\tau^+$  decays to leptons,  $\tau^+ \rightarrow l^+ \nu_l \bar{\nu}_\tau$ , ( $l = e, \mu$ ), denoted as tag side. The other is  $\tau^- \rightarrow K_S \pi^- \nu_\tau$  with  $K_S \rightarrow \pi^+ \pi^-$ , denoted as signal side. The charge conjugate decays are implied throughout the analysis unless specified.

Each charged track is required to satisfy the vertex requirement and detector acceptance in fast simulation. The events with four charged tracks and zero net-charge are required. The  $K_S$  candidates are selected from pairs of oppositely charged tracks, which satisfy a vertex-constrained fit to a common point. The two charged tracks with minimum  $\chi^2$  of vertex fit are assumed to be pions produced from  $K_S$ . The  $K_S$  is required to have an invariant mass in range  $0.485 < |M_{\pi^+\pi^-}| < 0.512 \text{ GeV}$ . Moreover, the flight significance of  $K_S$  candidates should be larger than 2. The decay length  $L$  of  $K_S^0$  for signal and backgrounds are shown in Fig. 1, and  $L > 0.5 \text{ cm}$  is further required to suppress the background events from  $\tau^- \rightarrow \pi^+ \pi^- \pi^- \nu_\tau$ .

For electron candidates,  $E/p$  is required to be larger than 0.8, where  $E$  is the deposited energy in the EMC and  $p$  is the momentum of the charged tracks. By default, muon candidates are selected according to the efficiency curve in fast simulation with following requirements:  $P(\mu) > 0.001$ ,  $P(\mu) > P(K)$  and  $P(\mu) > P(e)$  in the PID system, where  $P(X)$  is the probability of a candidate identified as particle  $X$ ,  $0.1 < E < 0.3 \text{ GeV}$

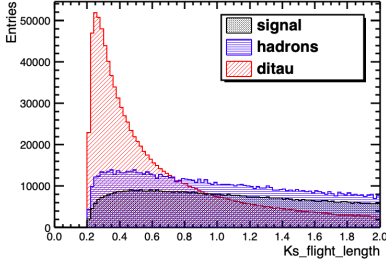


FIG. 1. The black, red and blue line represent signal process (signal),  $e^+e^- \rightarrow \tau^+\tau^-$  without signal processes (ditau) and hadronic final states  $e^+e^- \rightarrow q\bar{q}$  (hadrons), respectively. The x-axis unit is centimeter.

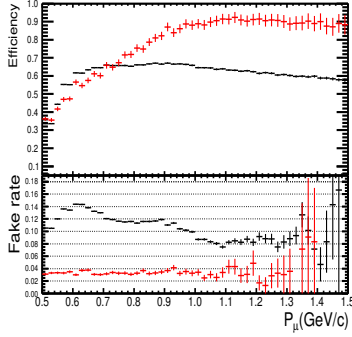


FIG. 2. Detection efficiency of muon and the mis-identification rate of  $\pi/\mu$ . The black dot is the response from reference detector in fast simulation, the red dot is the response from STCF R&D results in fast simulation.

in EMC, and layer requirement in MUD. The distribution of muon detection efficiency versus its momentum in fast simulation is shown as the black dots in Fig. 2. Besides, the fast simulation provides another function for muon selection from preliminary R&D results of STCF detector, where three kinds of  $\pi/\mu$  separation levels are provided, to be 3%, 1.7% and 1%, according to different requirement on  $\pi/\mu$  responses. The efficiency curve of STCF detector response is also shown in Fig. 2 in red dots on the basis of mis-identification rate to be 3%.

To suppress the background from  $\tau^- \rightarrow K_S\pi^-\pi^0\nu_\tau$  process, the  $\pi^0$  is reconstructed by selecting two good photon and the event is rejected if the invariant mass of any two photons locate in the region between 0.115 and 0.15  $\text{GeV}/c^2$ . The good photon candidates are selected with the efficiency sampled in fast simulation.

After above selection, the distribution of  $K_S\pi^-$  mass spectrum from generic MC is shown in Fig. 3(a), where there are huge backgrounds from  $e^+e^- \rightarrow \tau^+\tau^-$  with  $\tau$  decay inclusively, and the hadronic final states containing multiple  $\pi$  final states. The selection efficiency of signal and suppressing rate of backgrounds are listed in Table I.

Likelihood ratio  $y_L$  is used to suppress the backgrounds as introduced above. The likelihood ratio  $y_L(\vec{x})$  is defined

by

$$y_L(\vec{x}) = \frac{L_S(\vec{x})}{L_S(\vec{x}) + L_B(\vec{x})}, \quad (7)$$

where  $L_S$  and  $L_B$  are the likelihood function for signal and background event, respectively.  $\vec{x}$  is a set of variables used for likelihood. Each likelihood function  $L_{S/B}$  is the product of the probability density function(PDF) of the input variables defined by

$$L_{S/B} = \prod_{k=1}^{n_{var}} P_{S/B,k}(x_k), \quad (8)$$

where  $P_{S/B,k}$  is the signal/background PDF of the  $k$ -th input variable  $x_k$ . For this analysis, the set of variables  $\vec{x}$  includes the number of neutral clusters, the momentum of decay products of  $K_S$ , the decay length of  $K_S$ , the mass of  $K_S$ , the  $\chi^2$  of  $K_S$  in vertex fit, the  $E/p$  ratio of electron, the momentum of  $\mu$ , the cosine of the polar angle of  $\mu$ , the momentum of  $\pi$  and the momentum of  $K_S\pi^-$ . The polar angle mentioned above is defined as the angle between the track and the  $e^+e^-$  beam axis. The likelihood ratio  $y_L(\vec{x})$  from these variables between signal and backgrounds are shown in Fig. 4. The classifier requirement on  $y_L(\vec{x})$  is determined by optimizing the figure-of-merit  $\frac{S}{\sqrt{S+B}}$ , where S and B denotes the number of signal and backgrounds, to be 0.98. The mass spectrum of  $K_S\pi^-$  after above selections is shown in Fig. 3(b), and it is obvious that after likelihood requirement, the background has been significantly suppressed. The efficiencies with likelihood requirement are also shown in Table I.

The background events survived above selection come from hadronic final states or  $e^+e^- \rightarrow \tau^+\tau^-$  decay products, where  $e^+e^- \rightarrow \tau^+\tau^-$  is mainly from the final processes with one additional  $\pi^0$ , or multiple pion final states. At higher c.m. energies, the thrust  $T$  can be used to separate the hadronic final states from signal process, defined as

$$T \equiv \max_{\vec{n}} \frac{\sum_i |\vec{n} \cdot \vec{p}_i|}{\sum_i |\vec{p}_i|}, \quad (9)$$

where  $\vec{p}_i$  is the 3-momenta of the final state particles,  $\vec{n}$  is a 3-vector with unit norm. The typical distribution of thrust  $T$  at c.m. energy  $\sqrt{s} = 4.26$  and 7.0 GeV are shown in Fig. 5 between signal and hadronic processes. It is found that, the thrust  $T$  can provide a good distinguish between signal and hadronic background at high energy points such as  $\sqrt{s} = 7.0$  GeV. At lower c.m. energies, it is hard to distinguish the signal from background due to insufficient boost. However, with a good description of the hadronic final states from LUNDARLW, these background can be well described with MC simulation.

## V. OPTIMIZATION OF DETECTOR RESPONSE

After above selection criteria, the signal processes is selected with an efficiency of 22.2%, where the main



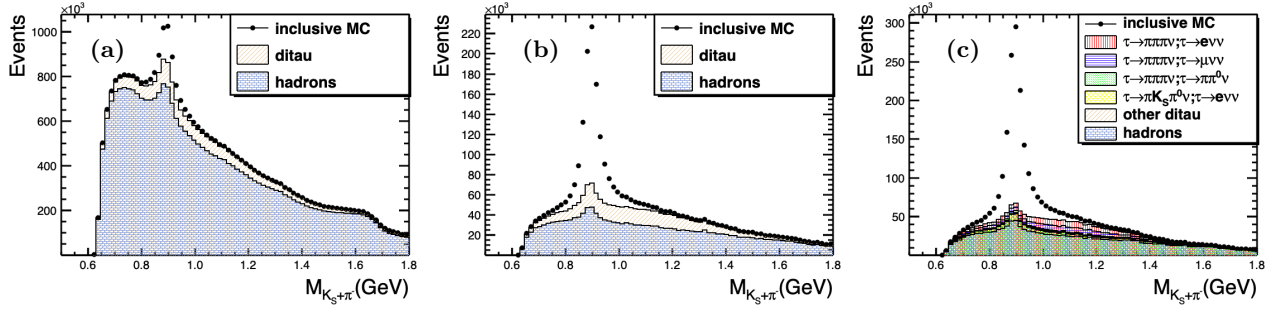


FIG. 3. Invariant mass of  $K_S\pi^-$  with combined  $e$ -tag and  $\mu$ -tag from  $\tau^+$  decay. (a) Distribution without detector optimization or likelihood requirement  $y_L$  (b) Distribution with likelihood requirement but no detector optimization (c) Distribution with likelihood requirement and detector optimization.

TABLE I. Signal and main backgrounds selection efficiency for the selection with neither detector optimization nor likelihood requirement  $\varepsilon_{\text{raw}}$ , with no detector optimization but applying likelihood requirement  $\varepsilon_{y_L}$ , with both detector optimization and likelihood requirement  $\varepsilon_{y_L \& \text{optimization}}$ .

Process	$\varepsilon_{\text{raw}}$ %	$\varepsilon_{y_L}$ %	$\varepsilon_{y_L \& \text{optimization}}$ %
$e^+e^- \rightarrow \tau^+\tau^-$ , $\tau^+ \rightarrow l^+\nu_l\bar{\nu}_\tau$ , $\tau^- \rightarrow K_S\pi^-\nu_\tau$	22.8	22.2	32.8
$e^+e^- \rightarrow \tau^+\tau^-$ (other than signal)	0.182	0.0403	0.0422
hadronic final states	0.304	0.0211	0.0179

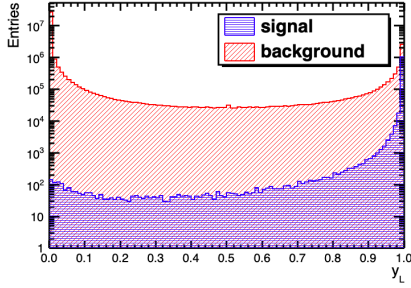


FIG. 4. Training and test samples distributed. The x-axis denotes  $y_L$  and y-axis which is set log scale denotes the entries. The signal labeled in figure is the process  $\tau \rightarrow \pi K_S \nu$ . The backgrounds are  $e^+e^- \rightarrow \tau^+\tau^-$  with  $\tau$  decay inclusively excluding the signal processes and the hadronic final states.

lose of the efficiency comes from the effects of tracking selection, secondary vertex fit of  $K_S$ , and the particle identification of leptons. These effects correspond to the sub-detectors of inner track, the PID system as well as the MUD. By studying the signal-to-background ratios for this process with variation of sub-detector's responses, the requirement of detector design can be optimized accordingly. With the help of fast simulation software package, four kinds of detector responses are studied as introduced below:

*a. Tracking efficiency* The tracking efficiency in fast simulation is characterized by two dimensions: transverse momentum  $P_T$  and polar angle  $\cos\theta$ , which are correlated with the level of track bending and the hit positions of tracks in the tracker system. For low-momentum track ( $P_T < 0.2$  GeV/c), it is hard to re-

construct efficiently due to stronger electromagnetic multiple scattering, electric field leakage, energy loss *etc.*. However, with different technique in inner track design at STCF, or with advanced track finding algorithm, there is improvement space for reconstruction efficiency of low-momentum track.

In this analysis, with the flexible approach to change the response of track reconstruction, the efficiency is scaled in the fast simulation, with a ratio from 1 to 1.4 at low momentum. For high momentum track, the efficiency keeps the same. The figure-of-merit, defined by  $\frac{S}{\sqrt{S+B}}$ , for the optimization of tracking efficiency is shown in Fig. 6, where  $S$  denotes signal yields of  $\tau \rightarrow K_S\pi\nu$ , and  $B$  denotes the backgrounds. From Fig. 6, it is found that the efficiency can be significantly improved with an optimization factor of 1.2.

*b. Momentum/position resolution* The resolution of momentum and position can also be optimized in fast simulation with proper functions. A better resolution will improve the significance of signal with no doubt. The effects of momentum and position resolutions on  $K_S$  reconstruction efficiency is also studied, and the position resolution is more sensitive than that of the momentum resolution for  $K_S$  reconstruction. Moreover, the position/momentum resolution for charged track has an improvement with an optimization factor of 0.5. It should be noted that in real case, these two resolutions are related with the same sources, which are the position resolution of a single wire in  $xy$  plane and  $z$  direction, and the multiple scattering.

*c.  $\pi/\mu$  separation* The default muon identification in fast simulation has a large  $\pi/\mu$  mis-identification rate as

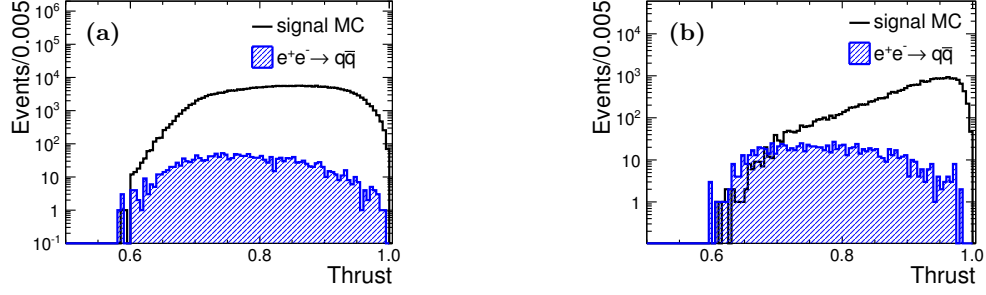


FIG. 5. The distribution of thrust  $T$  (log scale in y-axis) at c.m. energy (a)  $\sqrt{s} = 4.26$  GeV and (b)  $\sqrt{s} = 7.0$  GeV, line (in black) shows signal process and shaded histogram (in blue) shows hadronic processes.

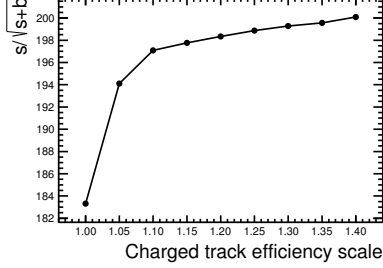


FIG. 6. The figure-of-merit for optimization of reconstruction efficiency for charged tracks.

shown with the black dots in Fig. 2. As the fast simulation provides the function for optimizing the  $\pi/\mu$  mis-identification, we can vary the mis-identification rate for  $\pi/\mu$  based on the provided efficiency curves. It is found that the significance can be significantly improved with better  $\pi/\mu$  mid-identification rate.

At STCF, the  $\pi/\mu$  separation power can be significantly improved with a hybrid design for MUD [47], and the efficiency curves are shown in Fig. 2 with red dots under the requirement of  $\pi/\mu$  mis-identification to be 3%. Three kinds of mis-identification rates are provided in STCF, with different efficiency for  $\mu$ , respectively. Table II gives the summarize of the selection efficiency for these three efficiency curves, where one can find, with the  $\pi/\mu$  mis-identification at 3%, the detector efficiency for signal process is the highest, this is because a moderate selection on the performance at MUD is applied with this requirement.

TABLE II. Efficiency of selecting  $\mu$  and final selection efficiency using STCF PID with different fake rate( $\pi/\mu$ ).

Fake rate( $\pi/\mu$ )/%	Eff. for $\mu$ /%	Eff. for bkg/%	Final eff./%
3	76.80	0.385	36.64
1.7	66.79	0.375	35.03
1	58.63	0.370	33.69

*d. Position/energy resolution for photon* In this analysis,  $\pi^0$  are vetoed to suppress the background with an additional  $\pi^0$ . The position and energy resolution for

neutral tracks are optimized with the fast simulation. With better detection for neutral tracks, the position and energy resolution is set to 6mm and 2.5%.

From above study, a set of optimization factors for sub-detector responses concerning this analysis is performed: the efficiency for charged track is improved by 20% at low momentum; the position/momentum resolution for charged track is improved by 50% compared with fast simulation by default; the  $\pi/\mu$  mis-identification rate is set at 3%. With these optimization factors applied, the signal selection efficiency is about 10% higher than with no optimization. The statistical sensitivity can be improved by  $1.3 \times 10^{-4}$  compared with no optimization. Moreover, the invariant mass of  $K_S\pi$  are shown in Fig. 3(c). The background level is significantly suppressed, where the dominant  $\tau$  pair decay background events are  $\tau^- \rightarrow \pi^+\pi^-\pi^-\nu_\tau$  and  $\tau^- \rightarrow K_S\pi^-\pi^0\nu_\tau$ . The optimized selection efficiency and the background level are summarized in Table I. The detailed selection efficiency for each step are listed in Table III, where the improvement of the selection efficiency comparing to the MC without optimization is given.

TABLE III. Cut flow for each selection criteria for signal processes, where  $\varepsilon$  is the overall efficiency,  $\varepsilon_{\text{rela}}$  is the relative efficiency for each criteria, and  $\Delta\varepsilon_{\text{rela}}$  is the relatively improvement of optimized detector response comparing to the original one.

Selection	$\varepsilon$ %	$\varepsilon_{\text{rela}}$ %	$\Delta\varepsilon_{\text{rela}}$ %
$N_{\text{charged\_track}}$	69.75	69.75	7.52
select $K_S$	54.34	77.90	13.1
lepton ID	37.89	87.31	19.13
$\pi$ ID	36.64	96.70	2.66
veto $\pi^0$	36.64	99.99	-
$K_S$ flight length	33.45	91.38	0.27
likelihood method	32.82	98.10	0.52
Total	32.82	-	-

## VI. STATISTICAL ANALYSIS

With above selection criteria and optimization procedure, the number of signal events  $\tau^-$  and  $\tau^+$  decay

mode in  $1 \text{ ab}^{-1}$  inclusive MC are obtained by fit the  $K_S\pi$  invariant mass with RooFit tool, where signal can be parameterized by the function as shown in Eq. (3) and background is described with simulated background. The efficiency corrected numbers for  $\tau^- \rightarrow K_S\pi^-\nu_\tau$  and  $\tau^+ \rightarrow K_S\pi^+\bar{\nu}_\tau$  are  $3681017 \pm 5034$  and  $3681127 \pm 5091$ , respectively. It shows a good consistency with input values. The statistical sensitivity of  $CP$  asymmetry with decay rate can be calculated according to Eq. (1), to be  $9.7 \times 10^{-4}$ .

Besides, the selection efficiency for this process with c.m. energy from  $\sqrt{s} = 4.0 \text{ GeV}$  to  $5.0 \text{ GeV}$  where the cross section for  $e^+e^- \rightarrow \tau^+\tau^-$  is the maximum, is studied as shown in Fig. 7. It is found that the efficiency

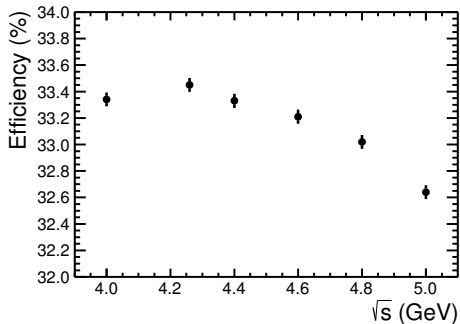


FIG. 7. Selection efficiencies for signal process at different c.m. energies from  $\sqrt{s} = 4.0 \text{ GeV}$  to  $5.0 \text{ GeV}$ .

is varying from 32.6% to 33.5% (without likelihood requirement), which is very stable in this energy region. Therefore, the statistical significance of signal process can be increased linearly with more data collected. Since it is not background free for this process, the sensitivity of  $CP$  asymmetry is proportional to the  $1/\sqrt{L}$ . Moreover, the sensitivity of  $CP$  asymmetry from  $0.1 \text{ ab}^{-1}$  to  $1 \text{ ab}^{-1}$  is shown in Fig. 8. With  $10 \text{ ab}^{-1}$

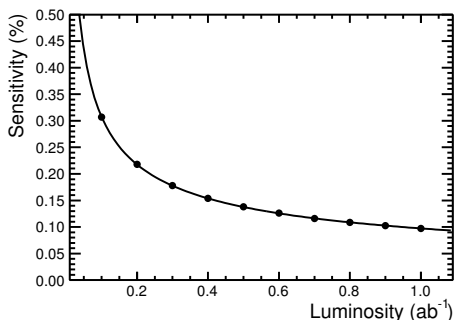


FIG. 8. The sensitivity of  $CP$  asymmetry from  $0.1 \text{ ab}^{-1}$  to  $1 \text{ ab}^{-1}$ .

integrated luminosity collected at STCF, the sensitivity

of the  $CP$  asymmetry is estimated to be  $3.1 \times 10^{-4}$ .

For systematic uncertainty, the possible sources of artificial CPV is the asymmetry of the  $\pi^\pm$  detection. The  $\pi^\pm$  detection asymmetry is caused by the different nuclear interaction cross section for  $\pi^+$  and  $\pi^-$  which can lead to a difference in tracking and PID efficiencies. Moreover, the detector induced asymmetry can be described by a function related to the momentum and polar angle of the particle and with the improvement of the measurement accuracy of the momentum and position resolution in STCF, the effect of correction on the measured CP asymmetry will be better than before.

## VII. SUMMARY AND PROSPECT

In this work, the sensitivity of decay rate asymmetry in  $\tau \rightarrow K_S\pi\nu$  decays is studied at  $\sqrt{s} = 4.26 \text{ GeV}$  with  $1 \text{ ab}^{-1}$  inclusive MC. Benefit from the largest cross section for  $e^+e^- \rightarrow \tau^+\tau^-$  at  $\sqrt{s} = 4.26 \text{ GeV}$ , to be  $3.5 \text{ nb}$ , and the optimized efficiency with fast simulation, the statistical sensitivity of  $CP$  asymmetry is 2.3 times improved comparing to that of BABAR [25], to be  $9.7 \times 10^{-4}$ . With  $10 \text{ ab}^{-1}$  luminosity collected at STCF in future, the sensitivity can be at a level of  $3.1 \times 10^{-4}$ , which is comparable to the uncertainty of theoretical prediction in the SM. A new round measurement of  $A_{CP}$  defined by the decay rate difference is important and desirable, c.f. (2), which will certainly shed light on the existence of the NP signal. Several theoretical models discussed in Sec. 2 will be reexamined. The  $CP$  asymmetry arose by the exchange of charged Higgs boson has also been explored in experiments, which is defined by the difference between angular observables, as a helpful complement. With such precision of  $10^{-4}$ , the remeasurement will be pursued, and all other prospects (form factors,  $|V_{us}|$  extraction etc.) could be furnished. Surprises could happen in the efforts hunting for  $CP$  violation and NP behind.

## ACKNOWLEDGMENTS

The authors thank the supercomputing center of USTC and Hefei Comprehensive National Science Center for their strong support. This work is supported by the Double First-Class university project foundation of USTC. The author XWK is supported by the National Natural Science Foundation of China under Project No.11805012, and the Fundamental Research Funds for the Central Universities.

[1] N. Cabibbo, Phys. Rev. Lett. **10**, 531 (1963).

[2] M. Kobayashi and T. Maskawa, Prog. Theor. Phys. **49**, 652 (1973).

- [3] H. Burkhardt *et al.* [NA31 Collaboration], Phys. Lett. B **206**, 169 (1988).
- [4] V. Fanti *et al.* [NA48 Collaboration], Phys. Lett. B **465**, 335 (1999).
- [5] A. Alavi-Harati *et al.* [KTeV Collaboration], Phys. Rev. Lett. **83**, 22 (1999).
- [6] B. Aubert *et al.* [BaBar Collaboration], Phys. Rev. Lett. **93**, 131801 (2004).
- [7] Y. Chao *et al.* [Belle Collaboration], Phys. Rev. Lett. **93**, 191802 (2004).
- [8] A. Poluektov *et al.* [Belle Collaboration], Phys. Rev. D **81**, 112002 (2010).
- [9] P. del Amo Sanchez *et al.* [BaBar Collaboration], Phys. Rev. D **82**, 072004 (2010).
- [10] R. Aaij *et al.* [LHCb Collaboration], Phys. Lett. B **712**, 203 (2012) Erratum: [Phys. Lett. B **713**, 351 (2012)].
- [11] R. Aaij *et al.* [LHCb Collaboration], Phys. Rev. Lett. **110**, no. 22, 221601 (2013).
- [12] R. Aaij *et al.* [LHCb Collaboration], Phys. Rev. Lett. **122**, no. 21, 211803 (2019).
- [13] A. D. Sakharov, Pisma Zh. Eksp. Teor. Fiz. **5**, 32 (1967).
- [14] M. E. Shaposhnikov, JETP Lett. **44** 465 (1986).
- [15] H. P. Nilles, Phys. Rept. **110**, 1 (1984).
- [16] H. E. Haber and G. L. Kane, Phys. Rept. **117**, 75 (1985).
- [17] W. Buchmuller, R. D. Peccei and T. Yanagida, Ann. Rev. Nucl. Part. Sci. **55** 311-355 (2005)
- [18] Y. S. Tsai, Nucl. Phys. Proc. Suppl. **55C**, 293 (1997);
- [19] I. I. Bigi, [arXiv:1204.5817](#) [hep-ph];
- [20] I. I. Bigi, Nucl. Phys. Proc. Suppl. **253-255**, 91 (2014);
- [21] E. Kou *et al.* [Belle-II], PTEP **2019** no.12, 123C01 (2019)
- [22] A. Pich, Prog. Part. Nucl. Phys. **75**, 41-85 (2014)
- [23] I. I. Bigi and A. I. Sanda, Phys. Lett. B **625**, 47 (2005).
- [24] Y. Grossman and Y. Nir, JHEP **1204**, 002 (2012).
- [25] J. P. Lees *et al.* [BaBar Collaboration], Phys. Rev. D **85**, 031102 (2012).
- [26] H. Z. Devi, L. Dhargyal and N. Sinha, Phys. Rev. D **90** no.1, 013016 (2014)
- [27] L. Dhargyal, LHEP **1** no.3, 9-14 (2018)
- [28] V. Cirigliano, A. Crivellin and M. Hoferichter, Phys. Rev. Lett. **120** no.14, 141803 (2018)
- [29] X. W. Kang, B. Kubis, C. Hanhart and U. G. Meißner, Phys. Rev. D **89**, 053015 (2014)
- [30] J. Rendon, P. Roig and G. Toledo, Phys. Rev. D **99** no.9, 093005 (2019)
- [31] F. Z. Chen, X. Q. Li, Y. D. Yang and X. Zhang, Phys. Rev. D **100** no.11, 113006 (2019)
- [32] A. Dighe, S. Ghosh, G. Kumar and T. S. Roy, [\[arXiv:1902.09561\]](#) [hep-ph].
- [33] I. I. Bigi, [arXiv:1204.5817](#) [hep-ph].
- [34] N. Mileo, K. Kiers and A. Szytnkman, Phys. Rev. D **91** no.7, 073006 (2015)
- [35] D. Kimura, K. Y. Lee and T. Morozumi, PTEP **2013** 053B03 (2013)
- [36] X. W. Kang and H. B. Li, Phys. Lett. B **684** 137-140 (2010), Int. J. Mod. Phys. A **26** 2523-2535 (2011), I. I. Bigi, X. W. Kang and H. B. Li, Chin. Phys. C **42**, no.1, 013101 (2018), X. D. Shi, X. W. Kang, I. Bigi, W. P. Wang and H. P. Peng, Phys. Rev. D **100** no.11, 113002 (2019)
- [37] G. Bonvicini *et al.* [CLEO Collaboration], Phys. Rev. Lett. **88**, 111803 (2002).
- [38] M. Bischofberger *et al.* [Belle Collaboration], Phys. Rev. Lett. **107**, 131801 (2011)
- [39] J. H. Kuhn and E. Mirkes, Z. Phys. C **56**, 661 (1992)
- [40] V. Bernard, JHEP **06**, 082 (2014)
- [41] R. Escribano, S. Gonzalez-Solis, M. Jamin and P. Roig, JHEP **09**, 042 (2014)
- [42] M. Jamin, J. A. Oller and A. Pich, Phys. Rev. D **74**, 074009 (2006)
- [43] D. Epifanov *et al.* [Belle], Phys. Lett. B **654**, 65-73 (2007)
- [44] H.-p. Peng, High Intensity Electron Positron Accelerator (HIEPA), Super Tau Charm Facility (STCF) in China, talk at Charm2018, Novosibirsk, Russia, May 21 - 25, 2018.
- [45] Q. Luo and D. Xu, Progress on Preliminary Conceptual study of HIEPA, a super tau-charm factory in China, talk at the 9th International Particle Accelerator Conference (IPAC 2018), held in Vancouver, British Columbia, Canada, April 29 - May 4, 2018.
- [46] Detector geometry management.
- [47] A fast simulation tool for STCF detector.
- [48] M. Ablikim *et al.* [BESIII Collaboration], Nucl. Instrum. Meth. A **614**, 345 (2010).
- [49] G. Balossini *et al.*, Nucl. Phys. B **758**, 227 (2006); G. Balossini *et al.*, Phys. Lett. B **663**, 209 (2008).
- [50] B. Andersson and H. Hu, [hep-ph/9910285](#).
- [51] S. Jadach, B. F. Ward and Z. Was, Comput. Phys. Commun. **130**, 260 (2000).
- [52] M. Tanabashi *et al.* [Particle Data Group], Phys. Rev. D **98**, 030001 (2018).
- [53] D. Epifanov *et al.* [Belle Collaboration], Phys. Lett. B **654**, 65 (2007)
- [54] L. Y. Dai, X. G. Wang and H. Q. Zheng, Commun. Theor. Phys. **57**, 841-848 (2012); [\[arXiv:1108.1451\]](#) [hep-ph]; Commun. Theor. Phys. **58**, 410-414 (2012)
- [55] L. Y. Dai and M. R. Pennington, Phys. Rev. D **90** no.3, 036004 (2014)
- [56] I. I. Bigi, X. W. Kang and H. B. Li, Chin. Phys. C **42** no.1, 013101 (2018)
- [57] X. D. Shi, X. W. Kang, I. Bigi, W. P. Wang and H. P. Peng, Phys. Rev. D **100** no.11, 113002 (2019)
- [58] S. Gonzalez-Solis, A. Miranda, J. Rendon and P. Roig, Phys. Lett. B **804**, 135371 (2020)